

## Evidence for efficient long-range AGN jet feedback from the low redshift Lyman- $\alpha$ forest

MEGAN TAYLOR TILLMAN ,<sup>1</sup> BLAKESLEY BURKHART ,<sup>2,3</sup> STEPHANIE TONNESEN ,<sup>3</sup> SIMEON BIRD ,<sup>4</sup>  
 GREG L. BRYAN ,<sup>3,5</sup> DANIEL ANGLÉS-ALCÁZAR ,<sup>6,7</sup> ROMEEL DAVÉ ,<sup>8,9</sup> AND SHY GENEL ,<sup>3,10</sup>

<sup>1</sup>Department of Physics and Astronomy Rutgers University, 136 Frelinghuysen Rd, Piscataway, NJ 08854, USA

<sup>2</sup>Department of Physics and Astronomy, Rutgers University, 136 Frelinghuysen Rd, Piscataway, NJ 08854, USA

<sup>3</sup>Center for Computational Astrophysics, Flatiron Institute, 162 Fifth Avenue, New York, NY 10010, USA

<sup>4</sup>University of California, Riverside, 92507 CA, U.S.A.

<sup>5</sup>Department of Astronomy, Columbia University, 550 W 120th Street, New York, NY 10027, USA

<sup>6</sup>Department of Physics, University of Connecticut, 196 Auditorium Road, U-3046, Storrs, CT 06269-3046, USA

<sup>7</sup>Center for Computational Astrophysics, Flatiron Institute, 162 5th Ave, New York, NY 10010, USA

<sup>8</sup>Institute for Astronomy, University of Edinburgh, Royal Observatory, Edinburgh, EH9 3HJ, UK

<sup>9</sup>University of the Western Cape, Bellville, Cape Town 7535, South Africa

<sup>10</sup>Columbia Astrophysics Laboratory, Columbia University, 550 West 120th Street, New York, NY 10027, USA

### ABSTRACT

Active galactic nuclei (AGN) feedback models are generally calibrated to reproduce galaxy observables such as the stellar mass function and the bimodality in galaxy colors. We use variations of the AGN feedback implementations in the IllustrisTNG (TNG) and SIMBA cosmological hydrodynamic simulations to show that the low redshift Lyman- $\alpha$  forest provides powerful independent constraints on the impact of AGN feedback. We show that TNG over predicts the number density of absorbers at column densities  $N_{\text{HI}} < 10^{14} \text{ cm}^{-2}$  compared to data from the Cosmic Origins Spectrograph (in agreement with previous work), and we demonstrate explicitly that its kinetic feedback mode, which is primarily responsible for galaxy quenching, has a negligible impact on the column density distribution (CDD) of absorbers. In contrast, we show that the fiducial SIMBA model including AGN jet feedback provides an excellent fit to the observed CDD of the  $z = 0.1$  Lyman- $\alpha$  forest across five orders of magnitude in column density. When removing the jet feedback mode in SIMBA we recover similar results as TNG, reminiscent of the ionizing “photon underproduction crisis”, a problem which arose from simulations lacking efficient heating/ionization of intergalactic medium (IGM) gas on large scales. AGN jets in SIMBA are high speed, collimated, weakly-interacting with the interstellar medium (via brief hydrodynamic decoupling) and heated to the halo virial temperature. Collectively these properties result in stronger long-range impacts on the IGM when compared to TNG kinetic feedback, which drives isotropic winds with lower velocities at the galactic radius. Our results suggest that the low redshift Lyman- $\alpha$  forest provides plausible evidence for long-range AGN jet feedback.

### 1. INTRODUCTION

The Ly $\alpha$  forest is a series of absorption line features that originate from the distribution of intergalactic gas along the line of sight to a background source. Those absorption lines provide a slew of statistical measurements including the flux PDF and power spectrum, column density distribution (CDD), and the widths of the absorption lines themselves (often referred to as b-values). This makes the Ly $\alpha$  forest a powerful diagnostic tool at high redshifts  $z \geq 2$  for the properties of dark matter (DM) and the thermal state of intergalactic medium (IGM) (Gunn & Peterson 1965; Palanque-Delabrouille et al. 2013; Viel et al. 2013; Puchwein et al. 2018; Bolton et al. 2021). The forest also provides a census of the

temperature and matter density at different epochs in the IGM (Altay et al. 2011; Rahmati et al. 2013; Hernquist et al. 1996; Hiss et al. 2018; Walther et al. 2019; Chabanier et al. 2020).

The absorbing gas that creates the forest is assumed to be in photoionization equilibrium with the ionizing background radiation, giving rise to a Ly $\alpha$  optical depth of  $\tau = -\ln F \propto N_{\text{H}}^2 T^{-0.7} \Gamma^{-1}$ , where  $F$  is the normalized transmitted flux,  $N_{\text{H}}$  is the hydrogen number density,  $T$  is the IGM gas temperature, and  $\Gamma$  is the hydrogen photoionization rate. While it is typical to assume photoionizing equilibrium, simulations differ in whether they assume thermal equilibrium. Thus, if the temperature is fully set by photoelectric heating by the integrated

ultraviolet (UV) emission from background stars and quasars, one may relate the statistics of the forest to the ultraviolet background (UVB) as well as to the underlying dark matter distribution. Indeed, the assumption of photoionization equilibrium in the IGM provides an excellent match to the observed properties of the Ly $\alpha$  forest at redshift  $z \geq 2$  (Katz et al. 1996; Hernquist et al. 1996) and allows for a quantitative connection between the Ly $\alpha$  forest and the dark matter density field (Weinberg & et al. 1999; Peebles et al. 2010).

Despite the vast utility the  $z \geq 2$  Ly $\alpha$  forest provides in constraining our conceptual understanding of the intergalactic medium (IGM), it has been difficult to reconcile simulations and models of the low redshift Ly $\alpha$  forest with observations. Observing the Ly $\alpha$  forest at  $z \leq 2$  requires state-of-the-art spectrographs, above Earth’s atmosphere, which reach the rest-frame far-ultraviolet (FUV) band (Danforth et al. 2016; Gurvich et al. 2017; Viel et al. 2017; Khaire et al. 2019; Christiansen et al. 2020). Observations with the Cosmic Origins Spectrograph (COS) aboard the Hubble Space Telescope, coupled with previous space missions in the UV such as FUSE (Danforth & Shull 2005), have enabled studies of the *low-redshift* Ly $\alpha$  forest in great statistical detail and with high sensitivity (Tripp et al. 2008; Meiring et al. 2011; Khaire et al. 2019; Danforth et al. 2016; Kim et al. 2020). In particular, Danforth et al. (2016) (henceforth D16) produced an extensive catalog of low redshift absorbers by building on previous HST catalogs. This catalog has enabled study of the low redshift forest in statistical detail previously impossible. The catalog contains over 5000 absorbers and probes column densities as low as  $N_{\text{H}} \approx 10^{12.5} \text{ cm}^{-2}$ . Confronted with the D16 dataset, cosmological hydrodynamical simulations struggled to reproduce the observed statistics of the low redshift Ly $\alpha$  forest. This disconnect, initially termed the “photon underproduction crisis” (PUC) (Kollmeier et al. 2014), led to a search for extra heating sources required to reproduce the observed neutral hydrogen levels in simulations.

Gurvich et al. (2017) was the first to point out that updated AGN feedback models were likely required to fully resolve the photon underproduction crisis and that AGN could provide additional heating beyond the standard UVB photoionization equilibrium models. Later studies continued to find that AGN feedback can have a dramatic heating effect on the IGM, especially at lower redshifts (Viel et al. 2017; Christiansen et al. 2020; Burkhardt et al. 2022).

In particular, Christiansen et al. (2020) explore variation runs of the SIMBA simulation that contain different implementations of AGN feedback. They explore

the properties of the IGM, with the main focus on the mean flux decrement, and find that the jet mode in particular is vital in reproducing what is observed at low redshift. In a similar vein, Burkhardt et al. (2022) found that the different AGN feedback models in the Illustris and IllustrisTNG (henceforth TNG) cosmological suites produced very different Ly $\alpha$  forest statistics (i.e. b-distribution, CDD, flux power spectrum), despite having the same UVB model. However the exploration of the entire column density range in the context of the SIMBA AGN jet feedback has not been conducted, and a comparison between the SIMBA and TNG CDDs would help disentangle the effects of AGN jet feedback modes.

By  $z = 0.1$  it has been shown that AGN feedback models can remake the entire thermal state of the IGM, including altering the hot gas and the neutral fraction (Martizzi et al. 2019). Thus the nature of the AGN model can be constrained not only by matching galaxy properties but also via observations of the IGM. In this work we focus directly on the CDD in the SIMBA cosmological suite used in Christiansen et al. (2020) to further investigate the proposed match of the Ly $\alpha$  forest produced by the SIMBA AGN jet model, with the Haardt & Madau (2012) UVB model, to the D16 dataset. We then compare to the TNG AGN kinetic feedback model and discuss differences that might cause the dramatically different CDD fits.

The paper is organized as follows: in Section 2 we briefly describe the simulations we analyze and how the Ly $\alpha$  forest spectra are generated and how column densities are calculated. In Section 3 we present the resulting  $z = 0.1$  column density distribution functions from various SIMBA simulations that include different AGN feedback models. We also do a comparison to the TNG simulation CDD presented in Burkhardt et al. (2022) and an additional TNG run that removes the kinetic AGN feedback mode. In Section 4 we discuss what these new statistics from SIMBA reveal about the AGN jet feedback, and we discuss differences between the TNG and SIMBA models that motivate the use of strong AGN jet feedback. Finally, we summarize and conclude in Section 5.

## 2. NUMERICAL SIMULATIONS

In this study we explore results from the SIMBA and IllustrisTNG (TNG) simulations. In this section we briefly describe these simulations and the AGN feedback models they implement. The original “fiducial” Simba and IllustrisTNG simulations are run in a 100 and 75 Mpc/h box respectively but in this study we explore “small box” runs that vary the AGN feedback physics in the simulations. This allows us to analyze the effects

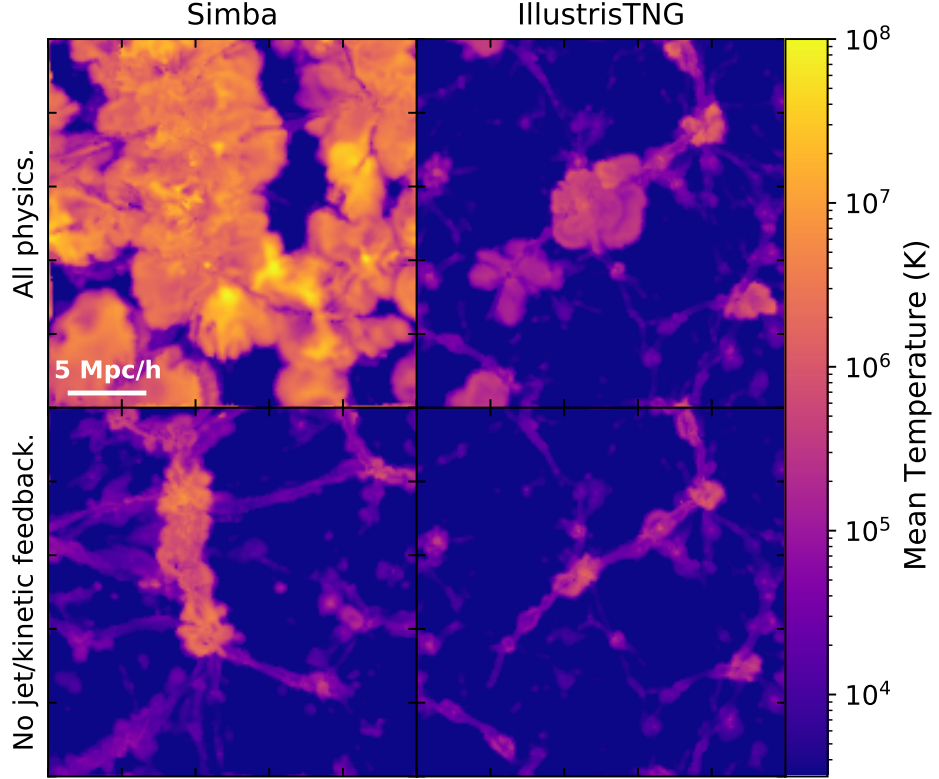


**Figure 1.** The  $z = 0.1$  mass weighted mean temperature projections for the SIMBA feedback variations and the CAMELS TNG runs. Each projection is over a depth of 525 kpc/h (corresponding to the absorber length discussed in section 2.4). The top rows display the fiducial runs and the bottom rows display the runs without AGN jet/kinetic feedback for SIMBA (left) and TNG (right). The SIMBA projection is a 25 by 25 Mpc/h portion of the full (50 by 50 Mpc/h) box while TNG is the full 25 by 25 Mpc/h box.

of the different AGN feedback models on the Ly $\alpha$  forest. We discuss more on these small box runs as compared to the fiducial simulation runs throughout this section. We discuss the resolution and box size of the simulations explored in this study and their effects on the CDD in the Appendix. In short, we find the CDD of the small box runs to be converged with the CDD of the fiducial simulations.

## 2.1. SIMBA

SIMBA is the next generation of the MUFASA cosmological galaxy formation simulations (Davé et al. 2016) run with GIZMO’s meshless finite mass hydrodynamics (Hopkins 2015), and employs a number of state of the art subgrid physical processes to form realistic galaxies. The GIZMO gravity solver is based on GADGET-3 (Springel et al. 2005) and evolves dark matter and gas together including gravity and pressure forces and follows shocks via a Riemann solver with no artificial viscosity. The SIMBA simulations use the following cosmological parameters:  $\Omega_m = 0.3$ ,  $\Omega_\Lambda = 0.7$ ,  $\Omega_b = 0.048$ ,  $H_0 = 68$  km/s/Mpc,  $\sigma_8 = 0.82$ , and  $n_s = 0.97$ . We briefly review

the essential aspects of the code here with a focus on the AGN model. For more details on these implementations we refer the reader to Davé et al. (2019).

Star formation is based on a Kennicutt–Schmidt Law (Kennicutt 1998) scaled by the H<sub>2</sub> fraction, which is calculated for each particle using its local column density and metallicity following Krumholz & Gnedin (2011). Galactic outflows are implemented as kinetic decoupled two-phase winds with an updated mass-loading factor based on particle tracking results from the Feedback in Realistic Environments (FIRE) zoom-in simulations (Anglés-Alcázar et al. 2017b). The production of 11 elements (H, He, C, N, O, Ne, Mg, Si, S, Ca, and Fe) are tracked from Type II and Ia supernovae and from stellar evolution. Relevant for the IGM, photoionization heating and radiative cooling are implemented using GRACKLE-3.1 (Smith et al. 2017) assuming ionization but not thermal equilibrium. GRACKLE assumes a Haardt & Madau (2012) ionizing background modified to account for self-shielding (Rahmati et al. 2013).

### 2.1.1. The Fiducial SIMBA AGN Feedback Model

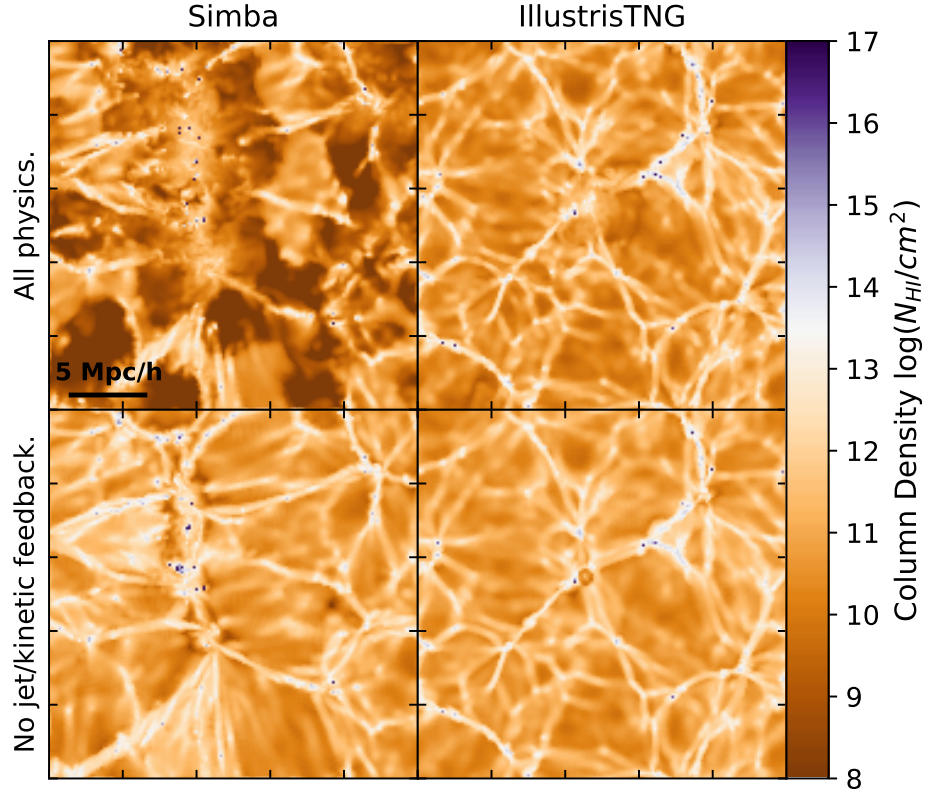


**Figure 2.** Same as Figure 1 but the Ly $\alpha$  column density projection over the 525 kpc/h slice. These projections show how rare column densities of  $\gtrsim 10^{15}$  cm $^{-2}$  are.

In the SIMBA simulations AGN feedback is modeled in two main discrete modes: a radiative mode at high Eddington ratios and a jet mode at low Eddington ratios (both implemented as kinetic outflows; [Anglés-Alcázar et al. 2017a](#)), with the latter accompanied by X-ray photon energy feedback ([Choi et al. 2012](#)).

The radiative mode drives multi-phase gas in winds at velocities of  $\sim 500 - 1500$  km/s. The transition to jet mode feedback occurs for SMBHs with Eddington ratios of  $\eta < 0.2$  and masses of  $M_{\text{BH}} \geq 10^{7.5} M_{\odot}$ . Full jet velocity is reached when  $\eta < 0.02$ . The gas ejected in these jets has a velocity that increases with lower  $\eta$  and higher  $M_{\text{BH}}$ , with a cap at 7000 km/s. This results in maximum wind speeds in the jet feedback mode of  $\sim 8000$  km/s when the appropriate criteria are met.

The gas ejected in jets is decoupled from the hydrodynamics and cooling for a timescale proportional to the Hubble time at the moment of ejection (this results in a decoupling of  $\sim 0.5$  Myr at  $z = 2.0$  to  $\sim 1.5$  Myr at  $z = 0$ ). As a result, the AGN jets can travel distances up to  $\sim 10$  kpc before their energy begins to be deposited. The temperature of the expelled gas in these jets is raised to the virial temperature of the halo ( $T_{\text{vir}} = 9.52 \times 10^7 (M_{\text{halo}}/10^{15} M_{\odot})^{1/3}$  K). The gas is also ejected in a purely bipolar highly collimated fash-

ion, along the angular momentum vector of the inner galactic disk.

X-ray feedback occurs in conjunction with jet feedback but only when the maximum 7000 km/s velocity increase occurs and the galaxy has a gas to stellar mass ratio of  $M_{\text{gas}}/M_{*} < 0.2$ . The X-ray feedback heats the non-ISM gas surrounding the SMBH accretion kernel. This heating decreases with distance to the black hole. For ISM gas, half of the X-ray energy is applied as kinetic energy in a radial outwards kick while the other half ends up as heat.

SMBH accretion in SIMBA includes two modes where cold rotationally supported gas accretes via a gravitational torque model ([Hopkins & Quataert 2011](#); [Anglés-Alcázar et al. 2017a](#)) while hot pressure supported gas follows the [Bondi \(1952\)](#) prescription. In both of these modes accretion is suppressed by a radiative efficiency of 0.1. The torque based accretion is capped at 3 times the Eddington limit while the Bondi accretion mode strictly follows the Eddington limit. Additionally SMBHs are limited to grow no more than 0.1% of their current mass in a single time step. The efficiency at which material is ejected in AGN winds is determined by the desired momentum input  $\dot{P}_{\text{out}} = 20L/c$  with  $L = 0.1\dot{M}_{\text{BH}}c^2$ . For a  $10^9 M_{\odot}$  SMBH ejecting gas at maximum velocities

this translates to an accreted mass to energy released conversion fraction of about 0.003 in the radiative mode or 0.03 in the jet mode. Additional information on the AGN feedback model can be found in Davé et al. (2019) and Christiansen et al. (2020).

### 2.1.2. Different SIMBA Runs

Along with the 100 Mpc/h box flagship run, additional SIMBA simulations were run where the AGN feedback modes were turned off, one at a time. These simulations enable us to isolate the impact of each feedback mode. Christiansen et al. (2020) explored these feedback variant simulations and found that the AGN jet feedback in particular is vital in reproducing IGM properties at low redshift. All of these additional simulations were run in a 50 Mpc/h box with  $2 \times 512^3$  resolution elements. The remaining properties of the simulations remain the same as the original full-size SIMBA run (apart from the variations in the AGN feedback).

Among the extra runs they explored, we utilize one for comparison in this study. The no-jet simulation removes the extra jet velocity boost from the AGN feedback so that the radiative feedback mode is the only AGN feedback present. Since the X-ray feedback only occurs in conjunction with the jet mode it is also removed from the no jet simulation. Christiansen et al. (2020) found negligible effects on the IGM when removing just the X-ray feedback, and we also found that removing X-ray feedback had a negligible effect on the CDD. When removing the radiative feedback, Christiansen et al. (2020) found little to no difference in the diffuse IGM at  $z = 0$ , and we confirm in this study that there is also no substantial difference in the CDD when removing AGN radiative feedback. As such, in this study we will focus on the no-jet variant and the all physics 50 Mpc/h box SIMBA run for comparison.

## 2.2. IllustrisTNG

The TNG suite consists of magnetohydrodynamic cosmological simulations which vary in mass resolution, volume, and complexity of the physics included (Pillepich et al. 2018a; Marinacci et al. 2018; Naiman et al. 2018; Springel et al. 2018; Nelson et al. 2018, 2019a; Pillepich et al. 2019; Nelson et al. 2019b). The simulations are performed with the AREPO code (Springel 2010; Weinberger et al. 2020) and gravitational interactions evolve via the TreePM algorithm (Springel et al. 2005). Radiative cooling from hydrogen and helium is implemented using the network described in Katz et al. (1996) and includes line cooling, free-free emission, and inverse Compton cooling. IllustrisTNG assumes ionization equilibrium and accounts for on-the-fly hydrogen column density shielding from the radiation background (Rahmati

et al. 2013). Metals and metal-line cooling are included (Vogelsberger et al. 2012, 2013) and star formation is implemented using the Springel & Hernquist (2003) sub-grid model.

In this paper we use a small box run of TNG from the CAMELS project which uses the same sub-grid models as the original IllustrisTNG simulations (Villaescusa-Navarro et al. 2021). We use this small box run instead of TNG100 since we compare to another small box run that removes the AGN kinetic feedback. Since each run has the same box size, resolution and initial conditions, it makes for simpler comparisons. These runs will be explained further in section 2.2.2.

### 2.2.1. TNG AGN Feedback

The AGN feedback in TNG has a high Eddington ratio thermal mode and a low Eddington ratio kinetic mode. In each mode the energy is directly deposited into the gas within the SMBH ‘feedback region’. The feedback region is a sphere around the SMBH with a size that scales with resolution  $\propto m_{baryon}^{-1/3}$ . The size of the feedback region is roughly constant within each simulation varying only slightly depending on the particles neighboring the SMBH. (Weinberger et al. 2017; Pillepich et al. 2018b).

The thermal mode deposits energy continuously as thermal energy. The kinetic mode is significantly more efficient than the thermal mode, as the pulsed injection of energy in the kinetic mode heats up the gas in the feedback region to higher temperatures (Weinberger et al. 2017). There is also a continually active radiative mode, which adds the SMBHs’ radiation flux to the cosmic ionizing background. However, the effect of the radiative mode on the halo is limited to the brightest AGN and is fairly small (Zinger et al. 2020).

The transition to the kinetic feedback mode happens for SMBHs with  $\eta < \chi$ , where

$$\chi = \min \left[ 0.002 \frac{M_{\text{BH}}}{10^8 M_{\odot}}, 0.1 \right]. \quad (1)$$

Thus, typically BHs with masses greater than  $M_{\text{BH}} \sim 10^8 M_{\odot}$  produce kinetic feedback. In this mode, energy is stored as the SMBH accretes gas until a minimum energy is reached ( $E_{\text{inj,min}} = 10\sigma_{DM}^2 m_{\text{enc}}$ , where  $\sigma_{DM}^2$  is the one-dimensional dark matter velocity dispersion around the SMBH and  $m_{\text{enc}}$  is the gas mass in the feedback region). Once the threshold is reached, energy is injected in a random direction as a momentum kick to the gas within the feedback region.

SMBH accretion in the TNG simulations uses the Bondi (1952) accretion prescription and is capped by the Eddington limit with a radiative efficiency of 0.2.

The efficiency fraction (at which accreted mass is converted into energy for the thermal mode) is a constant 0.02. In the kinetic mode the efficiency fraction is calculated as  $\rho/(0.05\rho_{\text{SFthresh}})$ , where  $\rho$  is the density of the gas around the SMBH and  $\rho_{\text{SFthresh}}$  is the star formation threshold density, but the efficiency fraction is capped at 0.2. See [Weinberger et al. \(2017\)](#) and [Zinger et al. \(2020\)](#) for more information on AGN feedback in TNG.

### 2.2.2. Different TNG Runs and CAMELS

For this study we explore small box TNG runs from the CAMELS project ([Villaescusa-Navarro et al. 2021](#)). These simulations use the same sub-grid models as TNG and are essentially small box runs with a resolution comparable to the original TNG300-1 simulation. Each CAMELS simulation has  $256^3$  gas resolution elements in a periodic comoving volume with a side length of 25 Mpc/h. The CAMELS project simulations are publicly available ([Villaescusa-Navarro et al. 2022](#)).

We utilize two runs from the CAMELS project. The first is the publicly available simulation that employs the same physics as TNG but in a smaller box. The second is the same except it removes the AGN kinetic feedback mode and is not publicly available. Together these runs allow us to analyze the effect of turning off the most efficient AGN feedback model in TNG as we do in the case of SIMBA.

### 2.3. AGN Models in TNG vs. SIMBA

Of the different AGN feedback modes modeled, the kinetic mode in TNG and jet mode in SIMBA are the most efficient feedback modes and thus most likely to affect the IGM (see Figure 1). While both modes are kinetic energy based and observationally motivated, they are vastly different in their implementation.

(1) The SIMBA jet mode hydrodynamically decouples, which allows the ejected gas to be deposited at some distance from the SMBH. By contrast, in TNG the kinetic energy of the jets is deposited in the region immediately around the SMBH.

A common struggle in cosmological simulations is ensuring outflows can reach the lower densities of the IGM, without over heating the gas, while also being able to match observed star formation rates within galaxies. The low numerical resolution of cosmological simulations can hamper galactic outflows, and without decoupling the outflows can be mostly quenched in high-mass galaxies ( $M_h \sim 10^{12} M_\odot/h$ , [Dalla Vecchia & Schaye 2008](#)). Decoupling in hydrodynamical simulations was first used for supernova feedback winds in [Springel & Hernquist \(2003\)](#). A momentum driven decoupled galactic outflow model has been found to successfully repro-

duce observed IGM carbon enrichment ([Oppenheimer & Davé 2006, 2008](#)). The SIMBA simulations included decoupling for the AGN jet feedback to mimic observed radio jets and to deposit their energy well outside the galaxy ([Davé et al. 2019](#)).

(2) The TNG kinetic mode stores energy for discrete feedback events while the SIMBA AGN feedback is instantaneous. Additionally, in TNG the ejection speed in the kinetic mode is affected by the energy ejected into the surrounding medium which depends on the minimum energy required for an event to take place. The jet speed at ejection depends on the energy ejected and the amount of mass being ejected, it is not explicitly set in the simulation. Conversely, the jet speed in SIMBA is explicitly set based on the instantaneous SMBH mass and the Eddington ratio.

(3) The jet feedback in SIMBA is collimated while the TNG kinetic feedback is isotropic. In SIMBA the ejection is bipolar occurring along the axis aligned with angular momentum vector of the gas in the BH kernel. In TNG the kinetic mode ejection occurs in a random direction that averages to isotropic over multiple events.

(4) The SIMBA simulations use a two mode accretion method while the TNG simulations use a single Eddington limited Bondi accretion mode. As a result SMBHs in SIMBA can accrete more mass in a time step than those in TNG. SIMBA limits SMBHs to grow no more than 0.1% of their current mass in any given time step. Additionally the efficiency at which accreted mass is converted into energy is different between SIMBA and TNG with SIMBA having a lower radiative efficiency fraction (0.1 in SIMBA and 0.2 in TNG).

(5) The SIMBA simulations heat AGN jets to the virial temperature of the host halo. The kinetic mode in TNG also heats up the gas ejected, occasionally beyond the virial temperature, but the temperature is not explicitly set as opposed to SIMBA.

In addition to the differences between the two feedback models, the UVB used in each simulation is also different. The UVB model also has an effect on the Ly $\alpha$  forest statistics so it must be considered here. SIMBA uses a modified version of the ([Haardt & Madau 2012](#)) UVB implemented using the GRACKLE framework ([Smith et al. 2017](#)) while TNG uses the [Faucher-Giguère et al. \(2009\)](#) UVB which has a larger UV photon density at  $z \sim 0.1$ .

### 2.4. Generating Column Densities

In this study we generate column density sightlines from the simulations using the publicly available *fake-*

*spectra* code outlined in Bird et al. (2015) and Bird (2017)<sup>1</sup>.

The neutral hydrogen column densities ( $N_{\text{HI}}$ ) from our generated sightlines are calculated for each pixel in units of neutral hydrogen atoms (HI)  $\text{cm}^{-2}$ . Column densities are computed by interpolating the neutral hydrogen mass in each gas element to the sightline using an SPH (smoothed particle hydrodynamics) kernel. The method used is based on the type of simulation; for the CAMELS TNG simulations a tophat (or uniform) kernel is used while for SIMBA a cubic spline kernel is used.

The column densities in 525 kpc/h slices are amalgamated into absorbers which are then used to calculate the column density distribution. This translates to absorbers of approximately 525 kpc/h in size. We find that defining the absorber size around 500 kpc/h results in a well converged CDD that simultaneously covers the smallest CD absorbers ( $N_{\text{HI}} \lesssim 10^{13} \text{ cm}^{-2}$ ) without slicing larger CD absorbers. Changing this value by a factor of 2 has a 10% or less effect on the CDD at column density values smaller than  $10^{12.5} \text{ cm}^{-2}$ . The CDD at column density values larger than  $10^{14} \text{ cm}^{-2}$  is insensitive to the choice of absorber size so long as that choice is not overly large.

We generate 5,000 sightlines randomly placed in each simulation box. We find this number of sightlines to be sufficient to avoid variations due to sampling. We note that at column densities of  $N_{\text{HI}} > 10^{15} \text{ cm}^{-2}$  variations in the CDDF will increase due to the rarity of those absorbers (see Figure 2), however observational error bars also become significantly larger.

### 3. RESULTS

Figures 1 and 2 show a mass weighted temperature projection and a column density projection respectively for the different simulations we study. These plots help illustrate the differences between the SIMBA and TNG simulations when disabling their most efficient AGN feedback mode. These projections are over a slice of thickness equal to the size of the absorber width we define in this study (525 kpc/h).

From the temperature projections it is clear that both the SIMBA and TNG AGN feedback models have an effect on the temperature distribution in the simulations. However the SIMBA jet feedback propagates much further through the simulation box than the kinetic mode feedback does in TNG.

In Figure 2, the column density projections demonstrate a clear difference between the SIMBA jet and no

jet runs but minimal difference is seen in the TNG simulations. From these projections alone we should expect to see a clear difference in the column density distribution function for the different SIMBA runs but minimal difference for the TNG runs.

The column density distribution function ( $f(N_{\text{HI}})$ ) is defined as

$$f(N_{\text{HI}}) = \frac{d^2 N_{\text{HI}}}{d \log(N_{\text{HI}}) dz} = \frac{F(N_{\text{HI}})}{\Delta N_{\text{HI}}} \Delta z \quad (2)$$

where  $F(N_{\text{HI}})$  is the fraction of absorbers with column densities in the range  $[N_{\text{HI}}, N_{\text{HI}} + \Delta N_{\text{HI}}]$ , and  $\Delta z$  is the redshift distance of the sightline. The CDDF then describes the number of absorbers within a logarithmic column density bin width and redshift distance.

The  $z = 0.1$  CDDFs produced for the various SIMBA and TNG simulations are presented in Figure 3 along with the D16 observational data. The data from the D16 catalog covers a redshift range of  $z = 0 - 0.47$  with 65% of the absorbers coming from the range  $z = 0 - 0.2$  and the median redshift for absorbers is  $z = 0.14$ . The simulated CDDF for both SIMBA and TNG are within  $1\sigma$  of the observational errors for redshifts  $0 < z < 0.2$  and within  $2\sigma$  for  $0 < z < 0.4$ . Therefore the redshift we have chosen to present in this study does not impact our main findings.

The main differences between the SIMBA and TNG results are the slope of the CDDF in the range  $10^{14} < N_{\text{HI}} < 10^{15} \text{ cm}^{-2}$  and the normalization at  $N_{\text{HI}} < 10^{14} \text{ cm}^{-2}$ . While the  $N_{\text{HI}} > 15 \text{ cm}^{-2}$  normalization of the fiducial TNG CDDF matches the observational data approximately, TNG tends to over-predict the number of lower column density absorbers (Burkhart et al. 2022,  $N_{\text{HI}} \lesssim 14^{10} \text{ cm}^{-2}$ ). *The SIMBA CDDF has an overall shallower slope and shows a remarkable match to the observations.*

In order to investigate the effect of the AGN jet mode we also overplot the CDDF of the no jet SIMBA simulation (black dashed line). The no jet SIMBA simulation shows dramatic differences from the fiducial SIMBA run (i.e. with jets) at all column densities. The main effect here is a re-normalization of the CDDF implying much more neutral hydrogen is present in the IGM.

### 4. DISCUSSION

We have found that the fiducial SIMBA run is an excellent match to the CDDF from D16. By comparison with the no-jet SIMBA run, we find that AGN jet feedback as implemented in SIMBA is a viable solution for the PUC. This is in agreement with Christiansen et al. (2020), but goes beyond the mean flux decrement (which is dominated by  $N_{\text{HI}} \sim 10^{13.7} \text{ cm}^{-2}$ ) to the full distribution of

<sup>1</sup> [https://github.com/sbird/fake\\_spectra](https://github.com/sbird/fake_spectra)

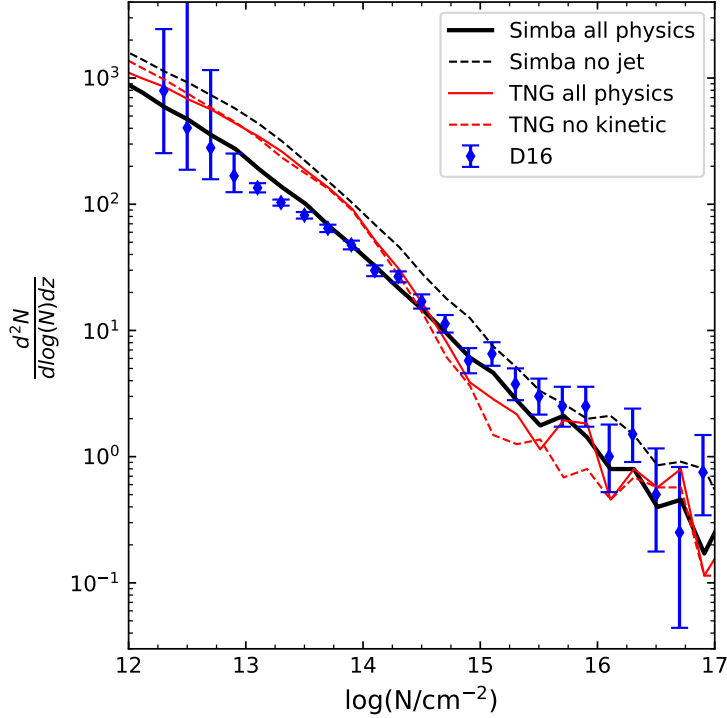


**Figure 3.** The  $z = 0.1$  CDDF for the SIMBA runs with and without the AGN jet feedback mode (black lines) and the CDDF for the IllustrisTNG runs with and without AGN kinetic feedback mode (red lines), compared to the D16 observational data (blue points). The solid black line is the fiducial SIMBA run, the dashed black line is the no jet feedback run, the solid red line is the fiducial CAMELS TNG run, and the dashed red line is the CAMELS TNG run without AGN kinetic feedback. The observational data is from Table 6 of D16.

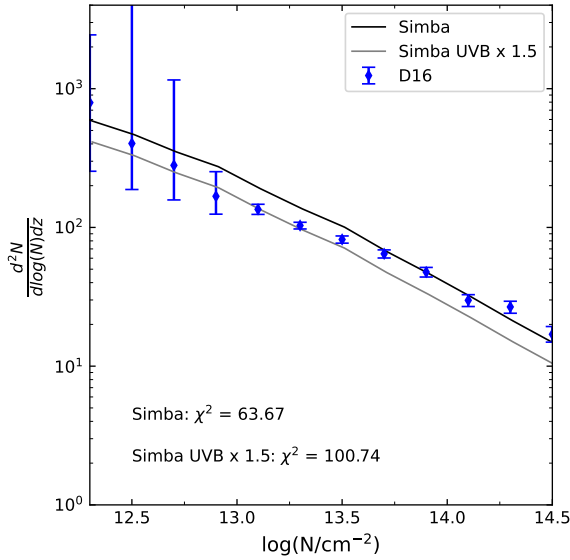


**Figure 4.** The  $z = 0.1$  CDDF of the fiducial SIMBA run and the same run corrected in post-processing to emulate the Faucher-Giguère (2020) UVB. Least squares values are included showing that the overall fit of the fiducial run is better than the corrected UVB fit despite the corrected UVB fit providing a better fit at the lowest CDs.

Ly $\alpha$ -forest absorbers. Christiansen et al. (2020) found that using the new Faucher-Giguère (2020) UVB background was required alongside jet feedback to fully solve the PUC when exploring *mean flux decrement* while we found that jet feedback alone is sufficient to match the observed *CDDF*.

We explore the CDDF with the updated (Faucher-Giguère 2020) UVB model using a post-processing UVB correction method. We follow the procedure outlined in Kollmeier et al. (2014) which uses the fact that  $N_{\text{HI}} \propto 1/\Gamma_{\text{HI}}$  where  $\Gamma_{\text{HI}}$  is the hydrogen photoionization rate. This method tends to slightly over predict the correction but is a good approximation and can be applied in post-processing. Regardless of the method used, updating the SIMBA UVB to utilize the Faucher-Giguère (2020) values will shift the CDD downwards since those rates are larger than the Haardt & Madau (2012) values at  $z = 0.1$ . The updated UVB in Faucher-Giguère (2020) has a hydrogen photoionization rate that is  $\sim 1.5$  times larger than the value used in the SIMBA simulations at  $z = 0.1$ . We calculate a  $\chi^2$  value using a least squares fit, in the CD range where this UVB correction method is most valid ( $N_{\text{HI}} \lesssim 14.5 \text{ cm}^{-2}$ ), to the observational data to compare the updated UVB fit to the fiducial run.

Looking at Figure 4, the updated UVB CDDF, with the Faucher-Giguère (2020) background, appears to match better at lower column densities ( $N_{\text{HI}} \lesssim 10^{13.5} \text{ cm}^{-2}$ ), but according to the  $\chi^2$  value the overall fit is worse than that of the fiducial run with the Haardt & Madau (2012) background. Since we explore the CDDF and not the mean flux decrement it is not surprising that our findings differ slightly from the Christiansen et al. (2020) results. Especially, the mean flux is dominated by column densities around  $N_{\text{HI}} \sim 10^{13.7} \text{ cm}^{-2}$  while the CDDF covers the full CD range.

We highlight that although kinetic feedback is included in both SIMBA and TNG, there remains a dramatic difference in their CDDF shapes. This indicates that the implementation of the jet feedback sub-grid model is important to the resulting Ly $\alpha$  forest statistics (as seen in Burkhardt et al. 2022, comparing Illustris to IllustrisTNG). When removing the jet feedback from SIMBA there is a subtle steepening of the CDDF slope at  $N_{\text{HI}} > 10^{14.5} \text{ cm}^{-2}$ , but the change is not enough to explain the large difference from the TNG slope around those CD values. While it remains difficult to determine the full extent of this difference at higher column densities ( $N_{\text{HI}} > 10^{15} \text{ cm}^{-2}$ ), it is likely that additional factors apart from AGN jet feedback are also influencing the value of the CDD slope.

We argue that the main reason SIMBA jet feedback affects the Ly $\alpha$  forest while TNG jets do not is the distance the AGN jets can travel. The decoupled AGN jets in SIMBA can travel up to  $\sim 10$  kpc before they begin to deposit their energy (Davé et al. 2019), which means these jets can bypass much of the ISM. Since the majority of the AGN jet energy can still be present by the time it reaches the CGM, it has a much higher likelihood of being able to propagate to affect the diffuse IGM. Zinger et al. (2020) found galaxies at the  $10^{10.5} M_{\odot}$  mass scale can produce kinetic feedback that not only heats up the ejected gas to temperatures beyond  $T_{\text{vir}}$  but that gas can also be completely removed from the galaxy. Despite this, the results from Figure 1 clearly show that energy from TNG kinetic feedback cannot propagate as far into the diffuse IGM as SIMBA jet feedback. Instead, TNG kinetic feedback largely affects the host galaxy and the more immediate surroundings.

The difference in AGN feedback efficiency between SIMBA and TNG can be seen from the temperature and column density projections (Figures 1 and 2). Heating from halos propagates further, in both SIMBA and TNG, when efficient kinetic feedback is enabled. However, heating from AGN does not reach as far in TNG as it does in SIMBA. Additionally, minimal effect is seen on the TNG column densities when adding/removing ki-

netic feedback, but a dramatic effect is seen for SIMBA when jet feedback is toggled.

While the column densities plotted in Figure 3 are all traditionally considered part of the Ly $\alpha$  forest, and assumed to be found largely in the IGM, the higher column densities ( $N_{\text{HI}} > 10^{13.5} \text{ cm}^{-2}$ ) tend to exist closer to and within halos/galaxies (Bouma et al. 2021) and the circumgalactic medium (CGM) (as in COS-Halos Werk et al. 2014; Prochaska et al. 2017). Therefore, the slope change at  $N_{\text{HI}} \sim 10^{14.5} \text{ cm}^{-2}$  when removing the jet feedback in SIMBA implies that with decoupling some jets may be capable of completely bypassing the material located within the host halo. Since the slope change is subtle the fraction of jets able to bypass the entirety of the halo would be small.

Looking at the maximum AGN jet speed further motivates the argument that SIMBA jets reach the diffuse IGM while TNG jets do not. SIMBA AGN outflows can reach maximum velocities of  $\sim 8000$  km/s (the outflow velocity in the radiative mode can reach up to  $\sim 1000$  km/s plus the 7000 km/s boost in jet mode) which is deposited as far as  $\sim 10$  kpc away from the point of ejection (Davé et al. 2019). Energy loss due to gravity results in a maximum velocity of  $\sim 7000$  km/s at the point energy begins to deposit.

The jet velocity at injection in TNG is not explicitly set but instead depends on the energy ejected and the amount of mass to which the momentum kick applies. Nelson et al. (2019a) found in post-processing analysis that TNG jets reach maximum velocities of  $\gtrsim 12,000$  km/s at time of injection (much higher than in SIMBA) but this reduces to  $\sim 3,000$  km/s at a distance of 10 kpc from the injection site. This is less than half the speed jets in SIMBA exhibit at a similar distance.

Another factor that could be reducing the distance that the TNG AGN feedback effects propagate to is the direction of ejection. TNG AGN jets are ejected in a random direction which averages to isotropic ejection over many events. Random directions that are more parallel to the galactic disk may reduce the overall distance that the AGN jet effects reach. In contrast, SIMBA jets are perfectly collimated along the direction of the angular momentum of gas within the black hole kernel. While this direction can change over time (depending on the angular momentum of accreting material), recurrent ejection of gas along a preferred direction can help maximize the long-range impact of AGN feedback.

In summary, from our comparison between the SIMBA fiducial and SIMBA no jet CDDFs, we find that jet feedback in SIMBA lowers the CDDF at all column densities, even the higher column densities associated with the CGM in halos (Werk et al. 2013). Therefore, the

jet feedback in SIMBA can re-couple to its surroundings close enough to the injection site to affect the CGM. Removing the kinetic feedback mode from TNG has a negligible effect on the CDDF implying that TNG jets are unable to reach/affect most if not all of the absorbers that make up the low  $z$  Ly $\alpha$  forest.

An important note is that the highest CDs ( $N_{\text{HI}} > 10^{15} \text{ cm}^{-2}$ ) should be subject to more scrutiny as these absorbers are less common and more likely to be affected by simulation box size and initial conditions. In the appendix we show these values to be converged between the original and small box simulations within  $1\sigma$  of the observational data. The TNG no kinetic feedback run at the higher CD ranges also appears converged with the original TNG100 simulation.

As it stands in this work, the TNG AGN kinetic feedback appears to have no effect on the low redshift Ly $\alpha$  forest. To truly disentangle AGN feedback effects on the neutral hydrogen in the TNG simulation one would need to study even higher CDs such as Lyman limit systems ( $10^{17} < N_{\text{HI}} < 10^{20} \text{ cm}^{-2}$ ) and damped Ly $\alpha$  absorbers ( $N_{\text{HI}} > 10^{20} \text{ cm}^{-2}$ ) in the jet vs no jet feedback TNG runs. However, obtaining a statistical sample of these types of absorbers at  $z < 0.5$  requires a larger box size.

The excellence of the SIMBA CDDF fit shows that the PUC can be solved by IGM heating from AGN jet feedback, rather than simply ionizing radiation. As seen in Figure 4, with highly efficient AGN jet feedback there is the potential of overheating the IGM when using stronger UVB models (i.e. [Faucher-Giguère 2020](#)). While AGN feedback can affect the IGM in ways the UVB cannot (i.e. the shape of the CDD as seen for SIMBA), future discussions of how AGN feedback is implemented in simulations should simultaneously consider how the AGN feedback is implemented and which UVB model to use in order to prevent over-heating the IGM.

It is also important to acknowledge that both the SIMBA and TNG simulations are in good agreement with the observed stellar mass function and specific star formation rate to stellar mass relation at lower redshifts ([Davé et al. 2020](#)). This emphasizes that an efficient AGN feedback model, when implemented carefully, can reproduce not only the observed intergalactic properties but the observed galactic properties as well.

Implementing strong AGN feedback in simulations has proved a difficult task in the past with a good example being the Illustris simulations ([Zinger et al. 2020](#)). The Illustris AGN feedback struggled to quench galaxies, resulting in stellar masses that were too high. The ‘bubble model’ in Illustris proved to eject high density gas too efficiently leading to low gas fractions and masses

for galaxies ([Genel et al. 2014](#)). Avoiding ejection of too much material from the ISM was one motivation for implementing decoupling to the SIMBA AGN feedback model.

## 5. CONCLUSIONS

We analyze the  $z = 0.1$  Ly $\alpha$  forest column density distribution function for the SIMBA and IllustrisTNG simulations to explore the effect of the different AGN jet feedback subgrid models. Additionally we analyze variations of these simulations that remove the jet feedback to determine the feedback’s effect on the CDDF and thus the IGM.

We confirm findings by [Christiansen et al. \(2020\)](#) that AGN jet feedback is vital to include in future cosmological hydrodynamic simulations as a solution to the photon underproduction crisis. We also support findings from [Berkhout et al. \(2022\)](#) that the precise implementation of the AGN feedback sub-grid model is a point worth considerable attention. Despite both SIMBA and TNG implementing observationally motivated models for AGN jet feedback, the SIMBA model matches the observed CDDF remarkably while TNG struggles with both slope and normalization offsets from the observed data.

Our main conclusions are as follows:

- The fiducial SIMBA cosmological simulations, which employ the [Haardt & Madau \(2012\)](#) UVB model and a three mode AGN feedback model with radiative, jet, and X-ray modes, has no photon underproduction crisis. The low redshift ( $z = 0.1$ ) Ly $\alpha$  forest CDDF in SIMBA matches HST COS data from D16.
- We confirm previous findings that turning off the AGN jet feedback mode recovers the PUC, and we conclude that AGN jets in SIMBA are able to inject heat and energy far away from the host halos and into the diffuse IGM. This is crucial to match the low  $z$  Ly $\alpha$  CDDF.
- We argue that the long-range AGN jets in SIMBA, which result from many variables in the AGN feedback model such as the decoupling, temperature and velocity of the ejected material, and collimation of the jets allow the feedback effects to reach the diffuse IGM and affect the Ly $\alpha$  forest. The TNG implementation of kinetic feedback results in ejections that are unable to reach the diffuse IGM and affect the Ly $\alpha$  forest CDD.
- We emphasise that the AGN feedback models should be built and implemented with the UVB

model utilized in mind. Despite the updated Faucher-Giguère (2020) UVB model providing a better fit for the SIMBA CDDF at  $N_{\text{HI}} \lesssim 13.5 \text{ cm}^{-2}$ , it produced an overall worse fit than the original SIMBA Haardt & Madau (2012) UVB CDDF. AGN jet feedback that is too efficient can risk over-heating the IGM when combined with a stronger UVB.

Since the precise implementation of jet feedback can have a dramatic effect on the low redshift Ly $\alpha$  forest statistics, exploring different subgrid models will be vital in constraining AGN feedback as a whole. We were not able to confidently infer the full reason for the slope difference between the SIMBA and TNG CDDF. We suspect the slope difference partially comes from the fact that TNG AGN jets do not reach as far as they can in the SIMBA simulations, but the change seen in SIMBA jet vs SIMBA no-jet does not fully explain the slope difference. Larger box runs (or additional runs with varying initial conditions) of the simulations where AGN jet feedback is turned off are likely necessary to fully converge the CDDF at the highest column densities and determine the full extent of the SIMBA slope changes. These runs could also reveal any effects missed when removing the TNG kinetic feedback mode.

It is likely important to explore the subtleties of specific simulations' sub-grid models in addition to comparing different simulation sub-grid models as a whole (e.g. investigate variations in the strength of TNG's AGN

feedback rather than comparing TNG to SIMBA). It is possible that the difference in the CDDF slope between IllustrisTNG and SIMBA could be explained by these subtleties. However, as a collection of simulations varying astrophysical parameters within the framework of different simulation suites, the CAMELS project is an excellent starting point for exploring the subtleties of different AGN feedback sub-grid models (Villaescusa-Navarro et al. 2021). Exploration of the AGN feedback parameters is revealing an interesting interplay between AGN and stellar feedback and their effect on the low redshift Ly $\alpha$  forest (Tillman et al. in prep). The exploration of AGN feedback parameters in CAMELS makes it a powerful tool for disentangling AGN feedback's role in solving the photon underproduction crisis.

<sup>1</sup> MTT thanks the Simons Foundation and the Center for Computation Astrophysics at the Flatiron Institute for providing the computational resources used for this analysis. BB is grateful for generous support by the David and Lucile Packard Foundation and Alfred P. Sloan Foundation. This work is supported by NASA Astrophysics Theory Program grant number 80NSSC22K0823. DAA acknowledges support by NSF grants AST-2009687 and AST-2108944, CXO grant TM2-23006X, and Simons Foundation award CCA-1018464. GLB acknowledges support from the NSF (AST-2108470, XSEDE grant MCA06N030), NASA TCAN award 80NSSC21K1053, and the Simons Foundation.

## APPENDIX

### A. RESOLUTION AND BOX SIZE

Figure 5 shows the CDD for the small-box SIMBA and TNG runs explored herein vs the original simulation runs. The small-box runs appear converged to the results of the full-box runs. The Ly $\alpha$  forest in TNG was studied in Burkhardt et al. (2022) and they found the CDD results to be converged for box sizes from 50 Mpc/h to 300 Mpc/h side lengths (at least up to  $N_{\text{HI}} \sim 10^{15} \text{ cm}^{-2}$ ). Figure 5 confirms the convergence of the SIMBA original 100 Mpc/h box size run and the small-box 50 Mpc/h run. The CAMELS TNG 25 Mpc/h box size run is converged with the original TNG100 run within  $1\sigma$  of the observational error bars. The resolution is an important factor in the convergence of the Ly $\alpha$  CDD with poor resolution leading to overall normalization shifts in the CDD that get worse with higher  $N_{\text{HI}}$  (Burkhardt et al. 2022). The resolutions in this study are sufficient as the normalization effect does not arise between the different runs.

## REFERENCES

- Altay, G., Theuns, T., Schaye, J., Crighton, N. H. M., & Dalla Vecchia, C. 2011, ApJL, 737, L37, doi: [10.1088/2041-8205/737/2/L37](https://doi.org/10.1088/2041-8205/737/2/L37)
- Anglés-Alcázar, D., Davé, R., Faucher-Giguère, C.-A., Özel, F., & Hopkins, P. F. 2017a, MNRAS, 464, 2840, doi: [10.1093/mnras/stw2565](https://doi.org/10.1093/mnras/stw2565)

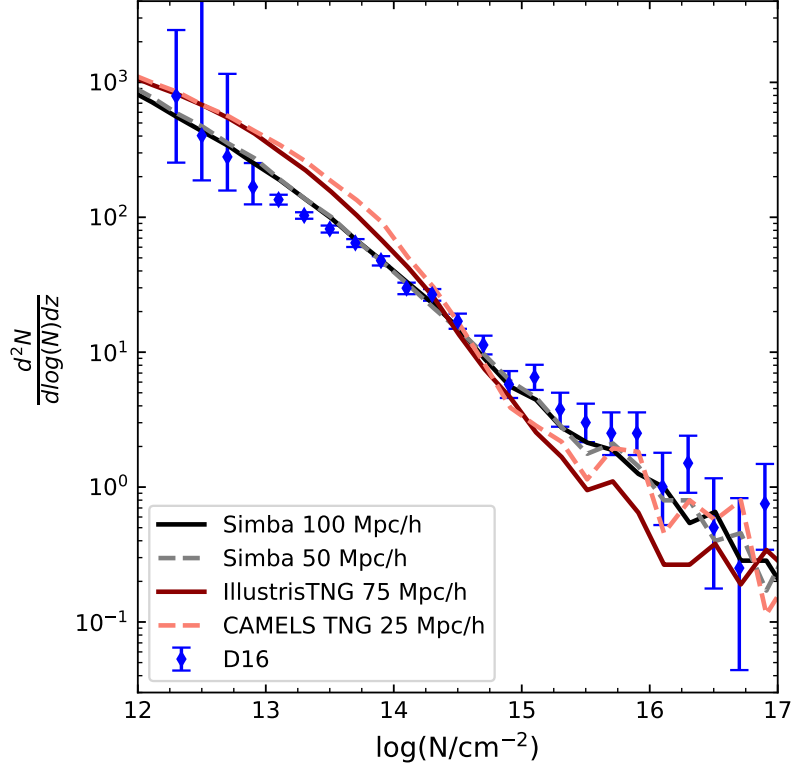


**Figure 5.** The  $z = 0.1$  CDDF for the original SIMBA and TNG runs vs the small box runs studied in this work. The results are converged exhibiting that the box size and resolution of these runs are converged for the Ly $\alpha$  statistics presented within this study.

Anglés-Alcázar, D., Faucher-Giguère, C.-A., Quataert, E., et al. 2017b, MNRAS, 472, L109, doi: [10.1093/mnrasl/slx161](https://doi.org/10.1093/mnrasl/slx161)

Bird, S. 2017, FSFE: Fake Spectra Flux Extractor. <http://ascl.net/1710.012>

Bird, S., Haehnelt, M., Neeleman, M., et al. 2015, MNRAS, 447, 1834, doi: [10.1093/mnras/stu2542](https://doi.org/10.1093/mnras/stu2542)

Bolton, J. S., Gaikwad, P., Haehnelt, M. G., et al. 2021, Limits on non-canonical heating and turbulence in the intergalactic medium from the low redshift Lyman-alpha forest. <https://arxiv.org/abs/2111.09600>

Bondi, H. 1952, MNRAS, 112, 195, doi: [10.1093/mnras/112.2.195](https://doi.org/10.1093/mnras/112.2.195)

Bouma, S. J. D., Richter, P., & Wendt, M. 2021, A&A, 647, A166, doi: [10.1051/0004-6361/202039786](https://doi.org/10.1051/0004-6361/202039786)

Burkhart, B., Tillman, M., Gurvich, A. B., et al. 2022, The Astrophysical Journal Letters, 933, L46, doi: [10.3847/2041-8213/ac7e49](https://doi.org/10.3847/2041-8213/ac7e49)

Chabrier, S., Bournaud, F., Dubois, Y., et al. 2020, MNRAS, 495, 1825, doi: [10.1093/mnras/staa1242](https://doi.org/10.1093/mnras/staa1242)

Choi, E., Ostriker, J. P., Naab, T., & Johansson, P. H. 2012, ApJ, 754, 125, doi: [10.1088/0004-637X/754/2/125](https://doi.org/10.1088/0004-637X/754/2/125)

Christiansen, J. F., Davé, R., Sorini, D., & Anglés-Alcázar, D. 2020, MNRAS, 499, 2617, doi: [10.1093/mnras/staa3007](https://doi.org/10.1093/mnras/staa3007)

Dalla Vecchia, C., & Schaye, J. 2008, MNRAS, 387, 1431, doi: [10.1111/j.1365-2966.2008.13322.x](https://doi.org/10.1111/j.1365-2966.2008.13322.x)

Danforth, C. W., & Shull, J. M. 2005, ApJ, 624, 555, doi: [10.1086/429285](https://doi.org/10.1086/429285)

Danforth, C. W., Keeney, B. A., Tilton, E. M., et al. 2016, ApJ, 817, 111, doi: [10.3847/0004-637X/817/2/111](https://doi.org/10.3847/0004-637X/817/2/111)

Davé, R., Anglés-Alcázar, D., Narayanan, D., et al. 2019, MNRAS, 486, 2827, doi: [10.1093/mnras/stz937](https://doi.org/10.1093/mnras/stz937)

Davé, R., Crain, R. A., Stevens, A. R. H., et al. 2020, MNRAS, 497, 146, doi: [10.1093/mnras/staa1894](https://doi.org/10.1093/mnras/staa1894)

Davé, R., Thompson, R., & Hopkins, P. F. 2016, MNRAS, 462, 3265, doi: [10.1093/mnras/stw1862](https://doi.org/10.1093/mnras/stw1862)

Faucher-Giguère, C.-A. 2020, MNRAS, 493, 1614, doi: [10.1093/mnras/staa302](https://doi.org/10.1093/mnras/staa302)

Faucher-Giguère, C.-A., Lidz, A., Zaldarriaga, M., & Hernquist, L. 2009, ApJ, 703, 1416, doi: [10.1088/0004-637X/703/2/1416](https://doi.org/10.1088/0004-637X/703/2/1416)

Genel, S., Vogelsberger, M., Springel, V., et al. 2014, MNRAS, 445, 175, doi: [10.1093/mnras/stu1654](https://doi.org/10.1093/mnras/stu1654)

Gunn, J. E., & Peterson, B. A. 1965, ApJ, 142, 1633, doi: [10.1086/148444](https://doi.org/10.1086/148444)

- Gurvich, A., Burkhardt, B., & Bird, S. 2017, ApJ, 835, 175, doi: [10.3847/1538-4357/835/2/175](https://doi.org/10.3847/1538-4357/835/2/175)
- Haardt, F., & Madau, P. 2012, ApJ, 746, 125, doi: [10.1088/0004-637X/746/2/125](https://doi.org/10.1088/0004-637X/746/2/125)
- Hernquist, L., Katz, N., Weinberg, D. H., & Miralda-Escudé, J. 1996, ApJ, 457, L51, doi: [10.1086/309899](https://doi.org/10.1086/309899)
- Hiss, H., Walther, M., Hennawi, J. F., et al. 2018, ApJ, 865, 42, doi: [10.3847/1538-4357/aada86](https://doi.org/10.3847/1538-4357/aada86)
- Hopkins, P. F. 2015, MNRAS, 450, 53, doi: [10.1093/mnras/stv195](https://doi.org/10.1093/mnras/stv195)
- Hopkins, P. F., & Quataert, E. 2011, MNRAS, 415, 1027, doi: [10.1111/j.1365-2966.2011.18542.x](https://doi.org/10.1111/j.1365-2966.2011.18542.x)
- Katz, N., Weinberg, D. H., & Hernquist, L. 1996, The Astrophysical Journal Supplement Series, 105, 19, doi: [10.1086/192305](https://doi.org/10.1086/192305)
- Kennicutt, Robert C., J. 1998, ApJ, 498, 541, doi: [10.1086/305588](https://doi.org/10.1086/305588)
- Khaire, V., Walther, M., Hennawi, J. F., et al. 2019, MNRAS, 486, 769, doi: [10.1093/mnras/stz344](https://doi.org/10.1093/mnras/stz344)
- Kim, T.-S., Wakker, B. P., Nasir, F., et al. 2020, Monthly Notices of the Royal Astronomical Society, 501, 5811, doi: [10.1093/mnras/staa3844](https://doi.org/10.1093/mnras/staa3844)
- Kollmeier, J. A., Weinberg, D. H., Oppenheimer, B. D., et al. 2014, ApJ, 789, L32, doi: [10.1088/2041-8205/789/2/L32](https://doi.org/10.1088/2041-8205/789/2/L32)
- Krumholz, M. R., & Gnedin, N. Y. 2011, ApJ, 729, 36, doi: [10.1088/0004-637X/729/1/36](https://doi.org/10.1088/0004-637X/729/1/36)
- Marinacci, F., Vogelsberger, M., Kannan, R., et al. 2018, MNRAS, 476, 2476, doi: [10.1093/mnras/sty397](https://doi.org/10.1093/mnras/sty397)
- Martizzi, D., Vogelsberger, M., Artale, M. C., et al. 2019, MNRAS, 486, 3766, doi: [10.1093/mnras/stz1106](https://doi.org/10.1093/mnras/stz1106)
- Meiring, J. D., Tripp, T. M., Prochaska, J. X., et al. 2011, ApJ, 732, 35, doi: [10.1088/0004-637X/732/1/35](https://doi.org/10.1088/0004-637X/732/1/35)
- Naiman, J. P., Pillepich, A., Springel, V., et al. 2018, MNRAS, 477, 1206, doi: [10.1093/mnras/sty618](https://doi.org/10.1093/mnras/sty618)
- Nelson, D., Pillepich, A., Springel, V., et al. 2018, MNRAS, 475, 624, doi: [10.1093/mnras/stx3040](https://doi.org/10.1093/mnras/stx3040)
- . 2019a, MNRAS, 490, 3234, doi: [10.1093/mnras/stz2306](https://doi.org/10.1093/mnras/stz2306)
- Nelson, D., Springel, V., Pillepich, A., et al. 2019b, Computational Astrophysics and Cosmology, 6, 2, doi: [10.1186/s40668-019-0028-x](https://doi.org/10.1186/s40668-019-0028-x)
- Oppenheimer, B. D., & Davé, R. 2006, MNRAS, 373, 1265, doi: [10.1111/j.1365-2966.2006.10989.x](https://doi.org/10.1111/j.1365-2966.2006.10989.x)
- . 2008, MNRAS, 387, 577, doi: [10.1111/j.1365-2966.2008.13280.x](https://doi.org/10.1111/j.1365-2966.2008.13280.x)
- Palanque-Delabrouille, N., Yèche, C., Börde, A., et al. 2013, AAP, 559, A85, doi: [10.1051/0004-6361/201322130](https://doi.org/10.1051/0004-6361/201322130)
- Peeples, M. S., Weinberg, D. H., Davé, R., Fardal, M. A., & Katz, N. 2010, MNRAS, 404, 1295, doi: [10.1111/j.1365-2966.2010.16384.x](https://doi.org/10.1111/j.1365-2966.2010.16384.x)
- Pillepich, A., Nelson, D., Hernquist, L., et al. 2018a, MNRAS, 475, 648, doi: [10.1093/mnras/stx3112](https://doi.org/10.1093/mnras/stx3112)
- Pillepich, A., Springel, V., Nelson, D., et al. 2018b, MNRAS, 473, 4077, doi: [10.1093/mnras/stx2656](https://doi.org/10.1093/mnras/stx2656)
- Pillepich, A., Nelson, D., Springel, V., et al. 2019, MNRAS, 490, 3196, doi: [10.1093/mnras/stz2338](https://doi.org/10.1093/mnras/stz2338)
- Prochaska, J. X., Werk, J. K., Worseck, G., et al. 2017, The Astrophysical Journal, 837, 169, doi: [10.3847/1538-4357/aa6007](https://doi.org/10.3847/1538-4357/aa6007)
- Puchwein, E., Haardt, F., Haehnelt, M. G., & Madau, P. 2018, ArXiv e-prints. <https://arxiv.org/abs/1801.04931>
- Rahmati, A., Pawlik, A. H., Raičević, M., & Schaye, J. 2013, MNRAS, 430, 2427, doi: [10.1093/mnras/stt066](https://doi.org/10.1093/mnras/stt066)
- Smith, B. D., Bryan, G. L., Glover, S. C. O., et al. 2017, MNRAS, 466, 2217, doi: [10.1093/mnras/stw3291](https://doi.org/10.1093/mnras/stw3291)
- Springel, V. 2010, MNRAS, 401, 791, doi: [10.1111/j.1365-2966.2009.15715.x](https://doi.org/10.1111/j.1365-2966.2009.15715.x)
- Springel, V., Di Matteo, T., & Hernquist, L. 2005, MNRAS, 361, 776, doi: [10.1111/j.1365-2966.2005.09238.x](https://doi.org/10.1111/j.1365-2966.2005.09238.x)
- Springel, V., & Hernquist, L. 2003, MNRAS, 339, 289, doi: [10.1046/j.1365-8711.2003.06206.x](https://doi.org/10.1046/j.1365-8711.2003.06206.x)
- Springel, V., Pakmor, R., Pillepich, A., et al. 2018, MNRAS, 475, 676, doi: [10.1093/mnras/stx3304](https://doi.org/10.1093/mnras/stx3304)
- Tripp, T. M., Sembach, K. R., Bowen, D. V., et al. 2008, ApJS, 177, 39, doi: [10.1086/587486](https://doi.org/10.1086/587486)
- Viel, M., Haehnelt, M. G., Bolton, J. S., et al. 2017, MNRAS, 467, L86, doi: [10.1093/mnrasl/slx004](https://doi.org/10.1093/mnrasl/slx004)
- Viel, M., Schaye, J., & Booth, C. M. 2013, MNRAS, 429, 1734, doi: [10.1093/mnras/sts465](https://doi.org/10.1093/mnras/sts465)
- Villaescusa-Navarro, F., Anglés-Alcázar, D., Genel, S., et al. 2021, ApJ, 915, 71, doi: [10.3847/1538-4357/abf7ba](https://doi.org/10.3847/1538-4357/abf7ba)
- Villaescusa-Navarro, F., Genel, S., Anglés-Alcázar, D., et al. 2022, arXiv e-prints, arXiv:2201.01300. <https://arxiv.org/abs/2201.01300>
- Vogelsberger, M., Genel, S., Sijacki, D., et al. 2013, MNRAS, 436, 3031, doi: [10.1093/mnras/stt1789](https://doi.org/10.1093/mnras/stt1789)
- Vogelsberger, M., Sijacki, D., Kereš, D., Springel, V., & Hernquist, L. 2012, MNRAS, 425, 3024, doi: [10.1111/j.1365-2966.2012.21590.x](https://doi.org/10.1111/j.1365-2966.2012.21590.x)
- Walther, M., Oñorbe, J., Hennawi, J. F., & Lukić, Z. 2019, ApJ, 872, 13, doi: [10.3847/1538-4357/aaefad1](https://doi.org/10.3847/1538-4357/aaefad1)
- Weinberg, D., & et al. 1999, in Evolution of Large Scale Structure : From Recombination to Garching, ed. A. J. Banday, R. K. Sheth, & L. N. da Costa, 346. <https://arxiv.org/abs/astro-ph/9810142>
- Weinberger, R., Springel, V., & Pakmor, R. 2020, ApJS, 248, 32, doi: [10.3847/1538-4365/ab908c](https://doi.org/10.3847/1538-4365/ab908c)

- Weinberger, R., Springel, V., Hernquist, L., et al. 2017, MNRAS, 465, 3291, doi: [10.1093/mnras/stw2944](https://doi.org/10.1093/mnras/stw2944)
- Werk, J. K., Prochaska, J. X., Thom, C., et al. 2013, ApJS, 204, 17, doi: [10.1088/0067-0049/204/2/17](https://doi.org/10.1088/0067-0049/204/2/17)
- Werk, J. K., Prochaska, J. X., Tumlinson, J., et al. 2014, ApJ, 792, 8, doi: [10.1088/0004-637X/792/1/8](https://doi.org/10.1088/0004-637X/792/1/8)
- Zinger, E., Pillepich, A., Nelson, D., et al. 2020, MNRAS, 499, 768, doi: [10.1093/mnras/staa2607](https://doi.org/10.1093/mnras/staa2607)